

# Suppression of Tearing Modes by RF Current Condensation

A. H. Reiman and N. J. Fisch

Princeton Plasma Physics Laboratory, Princeton University, Princeton, New Jersey 08544, USA

(Dated: December 14, 2024)

Currents driven by rf (radio frequency) waves in the interior of magnetic islands can stabilize deleterious tearing modes in tokamaks. Present analyses of stabilization strategies assume that the deposition of rf power is unaffected by the presence of an island, implying that the current required to stabilize the island increases as its width increases. However, there is a threshold island width above which this assumption is significantly violated. Current then condenses in the island, with a threshold width above which there is a decrease in the required current, and a second threshold at which the condensation effect is dramatically enhanced, stabilizing larger islands with more efficient use of the driven current. Interestingly, there is a hysteresis effect above the second threshold that shrinks the island to smaller width. The current condensation near the island O-line also reduces the difficulty of aiming accurately the rf power deposition to align radially with the island center.

PACS numbers:

*Introduction:* Magnetic islands in tokamaks deteriorate confinement and trigger disruptions. They may be driven unstable by neoclassical tearing modes (NTMs) arising from a deficit of the bootstrap current in the island interior, which drives a destabilizing resonant component of the magnetic field. Theoretical calculations in the early 1980's predicted that resonant RF driven currents could stabilize tearing modes [1, 2]. The recognition in the late 1990's that bootstrap currents were driving tearing modes in hot, collisionless tokamak plasmas [3–6] led to increased theoretical work [7–11], to experimental demonstrations of stabilization [12–18], and to continuing intensive attention [19–37]. A variety of rf waves are used to drive current [38], but, for stabilizing the NTM, the most studied methods are electron cyclotron current drive (ECCD) [39] and lower hybrid current drive (LHCD) [40]. ITER is designed with ECCD stabilization of NTMs, with continued effort to model and improve this capability [23, 27, 28]. However, what is identified here is an rf current condensation effect, previously overlooked, which importantly can facilitate island stabilization.

Underlying present analyses for controlling magnetic island growth is the assumption that the local deposition of rf power is unaffected by the presence of the island, so that the current required to stabilize the island increases as its width increases. Islands must then be suppressed while they are still small, with nominal current deposition widths comparable to or smaller than the island width. However, the sensitivity of rf stabilization to radial misalignment relative to the island, which is particularly an issue for a small island and narrow current deposition, introduces the risk that island growth will exceed what is envisioned in the scenarios for stabilizing small islands. The stabilizing effect changes sign (becoming destabilizing) if the current deposition is displaced a distance  $0.5 \max(W_i, W_d)$  relative to the island center, where  $W_i$  is the island width and  $W_d$  is the width of the current deposition layer [24]. The radial location of the magnetic island can be shifted on a relatively short time scale by an event such as a sawtooth crash or a flake

entering the plasma. Hence, to avoid disruptions, an efficient means of stabilizing large islands must be found.

In fact, the stabilization of large islands is facilitated by the thermal insulation of islands, which, absent interior losses, such as radiation, leads to peaking of the electron temperature at the O-line, with the island boundary at the lowest temperature. For LHCD [1] and ECCD, for which rf power is absorbed most where the electron temperature is highest, the absorbed power and current then peak at the O-line. Moreover, such absorption causes the center to become hotter yet, with the feedback giving what we call the *rf current condensation* effect.

Importantly, the current condensation in the island improves the distribution of the driven current. The more efficient use of the driven current then means that larger islands than presently contemplated can be stabilized. Rather than a monotonic increase with  $W_i$  of the current required for stabilization, we find instead a threshold width above which there is a decrease in the required current, and a second threshold at which the condensation effect is dramatically enhanced. Moreover, there is a hysteresis effect above the second threshold that shrinks the island to smaller width. The condensation effect also reduces the difficulty of aiming the rf current deposition for accurate radial alignment with the island center.

*Current Required for Stabilization:* The effect of a bootstrap or rf driven current on a magnetic island is determined by the magnitude and sign of the resonant Fourier component of the current, which produces a resonant component of the magnetic field that either stabilizes or destabilizes the magnetic island, depending on its sign. (The quantity  $\Delta'$  used to measure the contribution to stabilization in the context of the *modified Rutherford equation* [1, 7, 21, 41] is proportional to the resonant Fourier component of the current.) The driven current,  $\mathbf{j}_d = j_d \mathbf{B}/B$ , is aligned with the magnetic field  $\mathbf{B}$ . It follows from  $\nabla \cdot \mathbf{j} = 0$  that  $j_d/B$  is constant on the flux surfaces inside and outside the island. The strongest contribution to the resonant Fourier component comes from the current density on flux surfaces near the O-line.

To obtain a quantitative measure of the rf driven current required for stabilization, we consider a conventional cylindrical model for the magnetic field,

$$\mathbf{B} = \nabla\psi \times \hat{z} - (kr/m)B_z\hat{\theta} + B_z\hat{z}, \quad (1)$$

where we can expand  $\psi$  about the rational surface as  $\psi = \psi_0''x^2/2 - \epsilon \cos(\zeta)$ ,  $\zeta = m\theta - kz$ , and  $\epsilon$  is a constant (the “constant-psi approximation”). (See e.g. Refs. [41, 42].) We calculate the total driven current required to produce a resonant Fourier component of a fixed magnitude,

$$\bar{I} \equiv \int_{-\infty}^{\infty} dx \oint d\zeta j_d \cos(m\zeta) / \int_{-\infty}^{\infty} dx \oint d\zeta j_d \cos(m\zeta). \quad (2)$$

The inverse of this is sometimes called the *stabilization efficiency* [7, 43–45]. To determine the effect of localization near the O-line, we take  $j_d$  to be a step function,  $j_d = 1$  for  $\rho < \rho_b$ ,  $j_d = 0$  for  $\rho > \rho_b$ , where we define a normalized radial flux coordinate,  $\rho^2 = \psi/2\epsilon + 1/2$ . Fig. 1 shows a plot of  $\bar{I}$  vs.  $\rho_b$ . In the absence of the rf current drive condensation effect, for  $W_d$  large,  $\bar{I} \approx 7W_d/W_i$  for modulated injection and  $\bar{I} \approx 8W_d^2/W_i^2$  for continuous injection [44, 45]. For  $W_d$  small,  $\bar{I} \gtrsim 2.5$  for both continuous and modulated injection [45]. However, we see from the figure that if the driven current is concentrated near the O-line,  $\bar{I} \approx 1$ , over  $2\frac{1}{2}$  times smaller.

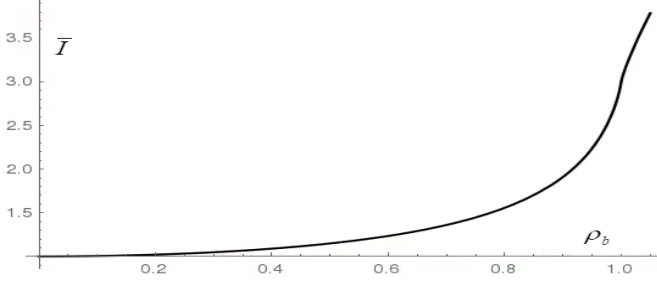


FIG. 1: Total driven current required to produce a fixed resonant Fourier component,  $\bar{I}$ , as a function of  $\rho_b$  for a step function current bounded by normalized flux  $\rho = \rho_b$ .

*Nonlinear rf Current Condensation:* Advantageously, rf heating in the thermally insulated island produces the nonlinear rf current condensation effect, where a temperature bump  $\Delta T$  produces wave absorption and current selectively at the O-line, enhanced by positive feedback. To see this, consider first for simplicity a slab model for a narrow island, which displays the same bifurcation behavior as the more accurate model. The temperature in the island typically equilibrates on a time scale short compared to the island growth time, so the steady-state heat diffusion can be put as

$$n\kappa_{\perp}\partial^2T/\partial r^2 = -P_{rf}, \quad (3)$$

where  $n$  is the density and  $\kappa_{\perp}$  is the perpendicular thermal diffusivity. We assume that the island is sufficiently large that the temperature can be taken to be constant

on the flux surfaces in the island interior [42, 46]. For simplicity, we take  $n$  and  $\kappa_{\perp}$  to be constant in the island.

Consider now lower hybrid waves or electron cyclotron waves, with resonant phase velocities parallel to the magnetic field between  $v_1$  and  $v_2 > v_1$ . Both for LHCD [47] and for ECCD [48], the power dissipated by an intense wave spectrum is exponentially sensitive to the lower resonant velocity. For simplicity, to model this sensitivity, we ignore both the depletion of the power and changes in the resonant parallel phase velocity along the ray trajectory. Thus, the sensitivity of the power dissipated on the temperature is captured by modeling the available power density  $P$  as constant in space, with the absorbed power density  $P_{rf}$  proportional to the local wave damping, i.e.,  $P_{rf} \propto \exp(-w_1^2)$ , where  $w_1 \equiv v_1/v_T$ ; the electron thermal velocity is defined by  $mv_T^2/2 = T$ ; and  $T$  is the electron temperature. While this crude model can be improved by ray tracing both for ECCD or LHCD [49–53], it captures the critical temperature dependency.

Write the temperature in the island as  $T = T_s + \tilde{T}(r)$ , where  $T_s$  is the temperature at the separatrix. The dissipated power can then be put as

$$P_{rf} \propto \exp(-w_1^2) = \exp(-w_{1s}^2) \exp(w_{1s}^2 \tilde{T}/T_s), \quad (4)$$

where  $w_{1s}$  is the value of  $w_1$  at the separatrix and we took  $\tilde{T}/T_s$  small, but  $w_{1s}^2 \tilde{T}/T_s$  not necessarily small. In the case of stiff transport [54–57], we require also  $\tilde{T}'/T_s'$  small, where  $T_s'$  is the temperature gradient at the rational surface in the absence of the island. With both limits satisfied, we can write  $P_{rf} = \bar{P}_0 \exp(w_{1s}^2 \tilde{T}/T_s)$ , where  $\bar{P}_0$  is constant in the island. Letting  $u \equiv w_{1s}^2 \tilde{T}/T_s$ ,  $P_0 \equiv W_i^2 w_{1s}^2 \bar{P}_0 / (4n\kappa_{\perp} T_s)$ , and  $x \equiv (r - r_r)/W_i$ , where  $r_r$  is the radial location of the rational surface and  $W_i$  is the island width, the diffusion equation becomes

$$u'' = -P_0 \exp(u), \quad (5)$$

where  $u''$  is the second derivative with respect to  $x$ .

We can solve Eq. (5) explicitly by multiplying by  $u'$  and integrating twice, giving

$$u(x) = \ln(\lambda_1/2P_0) - 2 \ln \left\{ \cosh \left[ \sqrt{\lambda_1} (x - \lambda_2)/2 \right] \right\},$$

where  $\lambda_1$  and  $\lambda_2$  are constants of integration to be determined by the boundary conditions. Imposing the boundary conditions that  $u' = 0$  at  $x = 0$  and  $u = 0$  at  $x = 1$ , we get the nonlinear eigenvalue equation

$$\lambda_1 = 2P_0 \cosh^2 \left( \sqrt{\lambda_1}/2 \right). \quad (6)$$

This nonlinear equation has two roots below a threshold in  $P_0$  corresponding approximately to  $P_0 = 0.88$ , and no roots above that threshold. This is a fold bifurcation. In the context of catastrophe theory, this type of behavior is known as a *fold catastrophe* [58].

The value of  $w_{1s}^2 \tilde{T}/T_s$  at  $x = 0$  as a function of  $P_0$  is shown as the inner dashed line (with the longer dashes)

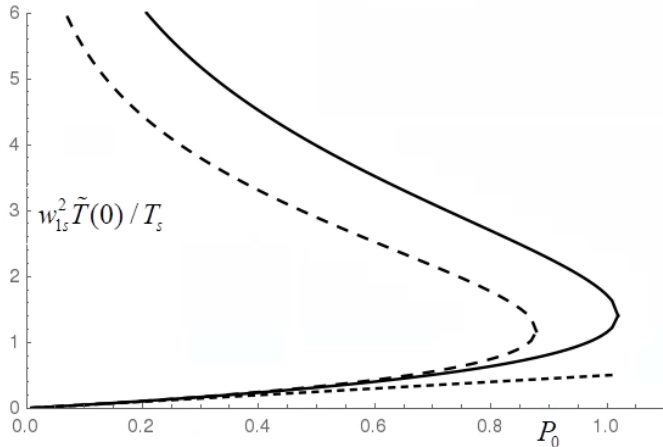


FIG. 2: Temperature differential  $w_{1s}^2 \tilde{T}(0)/T_s$  vs. normalized power density coefficient  $P_0$ , showing the fold bifurcation.

in Fig. 2. Above the threshold value of  $P_0$ , there is no steady-state solution for small  $\tilde{T}(0)/T_s$ . The temperature in the island continues to increase until it becomes large enough to encounter additional physics, which can be included in the nonlinear diffusion equation, leading to saturation of the temperature in the island, corresponding to an additional root of the modified steady-state diffusion equation. Possible candidates for the additional physics include the pinning of the temperature gradient at the threshold for stiff transport, the depletion of the energy in the rf wave, or energy loss due to radiation. The bifurcation should manifest under rf heating of fast electrons, with lower hybrid or electron cyclotron waves, even without unidirectional injection for current drive.

The bifurcated solution corresponds to the following physical picture. Initially, at low temperature, the power deposition term in the time-dependent heat diffusion equation dominates, and the temperature increases. The second derivative increases with increasing temperature, until it balances the power deposition at the lower root of the steady-state diffusion equation. A perturbation to a higher temperature gives a further increase in the second derivative, so that the lower root is stable. At sufficiently high temperature, the exponential begins to dominate, and the power deposition increases more rapidly with increasing temperature until the two terms again balance at the second root. The power deposition continues to increase more rapidly with increasing temperature, so that the second root is unstable. The temperature then continues to increase until limited by effects not considered here, giving a third, stable solution branch. The two lower solution branches merge at the bifurcation point. Above the bifurcation point the increase of the power deposition with temperature begins to dominate before a balance with the diffusive term is reached, and the temperature rises until the uppermost solution branch is reached. Interestingly, if the heating power is now decreased, there is a hysteresis effect, with the solution

moving along the uppermost branch, allowing this solution to be maintained at lower power levels. The solution should have a clearly identifiable experimental signature, with islands saturated at narrow widths.

The solid line in Fig. 2 corresponds to the solution for a more accurate treatment of the diffusion, taking into account the geometry of the island flux surfaces. For that treatment, we use the magnetic field of Eq. (1), we define  $\rho$  as before, and we transform our angular coordinate to  $\eta = \arcsin[\sin(\zeta/2)/\rho]$ . Defining an operator

$$\langle f \rangle(\rho) \equiv \int_{-\pi/2}^{\pi/2} \mathcal{J} f(\rho, \eta) d\eta, \quad (7)$$

where  $\mathcal{J} = (\nabla \rho \cdot \nabla \eta \times \nabla \phi)^{-1}$ , we can then write

$$\frac{d}{d\rho} \left( \left\langle |\nabla \rho|^2 \right\rangle \frac{d}{d\rho} T(\rho) \right) = \frac{1}{2\pi n \kappa_{\perp}} P_{rf}(\rho) \frac{dV}{d\rho}, \quad (8)$$

as our diffusion equation, where  $V(\rho)$  is the volume inside the corresponding flux surface. Discarding a term small in  $W_i/R$ , where  $R$  is the major radius, we get

$$\begin{aligned} \frac{d}{d\rho} \left( \frac{1}{\rho} [E(\rho) - (1 - \rho^2) K(\rho)] \frac{d}{d\rho} u(\rho) \right) \\ = P_0 \rho K(\rho) \exp(u), \end{aligned} \quad (9)$$

where  $K(k) \equiv \int_0^{\pi/2} (1 - k^2 \sin^2 \chi)^{-1/2} d\chi$  is the complete elliptic integral of the first kind, and  $E(k) \equiv \int_0^{\pi/2} (1 - k^2 \sin^2 \chi)^{1/2} d\chi$  is the complete elliptic integral of the second kind. We solve the equation with the boundary conditions  $u = 0$  at the separatrix and  $du/d\rho = 0$  at the O-point. The solution depends on the parameter  $P_0$ . The bifurcation threshold corresponds to  $P_0 \approx 1.02$ .

The bottom curve in Fig. 2 (with the smaller dashes) shows the solution of the linear diffusion equation, which neglects the dependence of the power deposition on the temperature. Even below the bifurcation threshold, the bottom branch of the solid curve in Fig. 2, shows that the effect of the exponential on the power deposition becomes important when that solution deviates from the linear one, and the exponential dependence of the rf driven current on the temperature perturbation then also becomes important, leading to the current condensation.

*Experimental Implications:* At the bifurcation threshold,  $w_1^2 \tilde{T}/T_s \approx 1.4$ . Estimating  $w_1^2 \approx 10$  gives  $\tilde{T}/T_s \approx 15\%$  at the bifurcation threshold. Tearing stabilization experiments via electron cyclotron waves on TEXTOR found  $\tilde{T}/T_s \approx 20\%$  [59], suggesting that the experiments may have approached or exceeded the bifurcation threshold. As discussed, one result of exceeding the bifurcation threshold would be the hysteresis effect, with the island suppressed to widths below what would otherwise be achievable. In fact, suggestively, the TEXTOR experiment observed suppression to widths well below the calculated widths of the power deposition profiles, where the stabilizing effect is predicted to be much reduced [60]. The condensation threshold, where the nonlinear solution

deviates from the linear one in Fig. 2, occurs at about half the bifurcation threshold, suggesting that TEXTOR was well above the condensation threshold.

The linear solution shown in Fig. 2 provides a useful benchmark, allowing us to make use of previous linear calculations to determine predicted bifurcation thresholds. The bifurcation threshold corresponds to the value of  $P_0$  at which the linear calculation finds  $w_1^2 \tilde{T}/T_s \approx 0.5$ , corresponding to  $\tilde{T}/T_s \approx 5\%$ . Solutions of the linear equation in Ref. [59] for the  $q = 2$  surface in ITER, assuming an island width of 24 cm, find  $\tilde{T}/T_s \approx 6\%$  under the assumption that the thermal diffusivity in the island is the same as that near the unperturbed rational surface, and  $\tilde{T}/T_s \approx 25\%$  if the thermal diffusivity is a factor of 6 smaller. There is, however, experimental evidence of strongly reduced transport in the interior of magnetic islands [61–63]. If the transport were reduced an order of magnitude relative to that outside the island, the bifurcation threshold island width in ITER would then be only about 8 cm, suggesting that the bifurcation, and the accompanying hysteresis effect, may be seen in ITER. The threshold for the current condensation effect would be reached for an island width of less than 6 cm, above which the ECCD stabilization would become more effective, providing some protection against uncontrolled island growth. These estimates do not take into account possible sources of heating in the islands other than ECH, which would lower the thresholds even further.

*Ohmic Current Condensation:* The Ohmic current  $J_{OH}$ , like the rf current  $J_{rf}$ , increases with  $\tilde{T}$ , and, therefore, will also condense at the O-line. Under normal operation, it is supportive of the total current, and so is also stabilizing. In an rf-driven discharge, the Ohmic current can be written as  $J_{OH} = J_{Sp} + J_H$ , where  $J_{Sp} = \sigma_{Sp} E$  is the Ohmic (Spitzer) current in the absence of the rf, and  $J_H = \sigma_H E$  is due to the *hot conductivity*  $\sigma_H$ , arising from electron velocity space distortions proportional to the rf power dissipated. The hot conductivity  $\sigma_H$  has been theoretically predicted [64] and experimentally verified in detail [65]. Since the Spitzer conductivity  $\sigma_{Sp}$  is proportional to  $T^{3/2}$ , we have for extra current density  $\Delta J$  due to temperature differential  $\Delta T = \tilde{T}(0)$

$$\Delta J_{Sp}/J_{Sp} = \Delta \sigma_{Sp}/\sigma_{Sp} = (3/2)\Delta T/T_s. \quad (10)$$

But since the hot conductivity  $\sigma_H$  is proportional to  $P_{rf}$ ,

$$\frac{\Delta J_H}{J_H} = \frac{\Delta \sigma_H}{\sigma_H} = \frac{\Delta P_{rf}}{P_{rf}} = w_1^2 \frac{\Delta T}{T_s} = \frac{\Delta J_{rf}}{J_{rf}}, \quad (11)$$

so that, like for the rf current, small temperature bumps produce a relative change in  $J_H$  larger by  $w_1^2 \gg 1$  than that in the Spitzer current  $J_{Sp}$ . For large  $w_1^2 \Delta T/T_s$ , this differential becomes exponentially larger. For usual tokamak operation, the hot conductivity current, is however, relatively small, so the main Ohmic current is the Spitzer current  $J_{Sp}$ . Now to stabilize the NTM requires  $J_{rf} \sim J_{BS}$ . It is expected that at the  $q = 2$  surface in ITER the bootstrap current density will be comparable

in magnitude to the Spitzer current density [66]. Thus, in the case of ITER, the extra Ohmic current condensation on the O-line caused by the temperature variation is small compared to the extra rf current.

*Hot Conductivity Destabilization Effect:* In contrast, the fast rise of  $\Delta J_H \sim w_1^2$  with  $w_1$  may play a critical role in the case of rf current overdrive. The *current overdrive* occurs when the rf is utilized for start-up operation [67–72], or when it is oscillated to optimize the current drive efficiency [73, 74]. The rf-driven current then exceeds the total toroidal current, inducing a toroidal electric field that opposes the rf-driven current, such that  $J_{OH} \simeq -J_{rf}$ . This is opposite to the case of supportive current drive, where the toroidal electric field supports the driven current. Now a change  $\Delta T$  at the O-line produces extra Ohmic current  $\Delta J_{OH}$  opposite to both the total current and the rf-driven current, and so is destabilizing rather than stabilizing. For strong overdrive, the Ohmic countercurrent is mainly limited by the hot conductivity, with  $J_{OH} \simeq J_H$  [64]. As opposed to the Spitzer current increment  $\Delta J_{Sp}$ ,  $\Delta J_H \sim w_1^2$ , so it strongly condenses on the O-line, nearly matching the rf incremental current  $\Delta J_{rf}$ , except that it is destabilizing. Moreover, any inadvertent rf power driving current opposite to  $J_{rf}$ , will further increase  $J_H$ . Some such power is inevitable both for LHCD and ECCD. The implications for NTM control are that it will be more difficult to stabilize the NTM in the rf overdrive mode in the limit where the overdrive is particularly strong, namely when the hot conductivity current is nearly equal to the rf-driven current, and when the rf current is produced by ECCD or LHCD. A weaker rf overdrive would reduce this destabilization effect.

*Comparison of Current Drive Methods:* Although other means of noninductive current drive have been contemplated for NTM stabilization, the current condensation effect described here is only available for ECCD and LHCD, because their damping decrements are highly sensitive to the electron temperature. This sensitivity is not available for current drive methods based on sub-thermal electrons [75], such as through Alfvén waves, for neutral beam current drive [76], even if it could be relatively localized through minority species heating [77].

Most of the experimentation to date has involved ECCD rather than LHCD, perhaps in part because of the thought that ECCD could be better localized. However, with current condensation on the O-line, this localization may no longer be critical. Moreover, launching lower hybrid waves from the tokamak high-field side allows greater localization through single-pass absorption, and also enables high-magnetic field compact tokamaks [78, 79]. In addition, available to LHCD, but not ECCD, is the opportunity to tap the energy in  $\alpha$  particles in a reactor through the  $\alpha$ -channeling effect [80]. The channeling is in fact most effective under high-field side launch [81, 82]. Thus, while both ECCD and LHCD advantageously exploit the current condensation effect, there may be a further advantage to LHCD in capturing  $\alpha$ -particle energy in tokamak reactors while stabilizing the NTM.

*Summary and Conclusions:* The rf-driven current condensation effect identified here increases the efficiency of rf current drive stabilization, with heat insulation producing a narrower power deposition profile, centered exactly on the O-line, which is further self-consistently narrowed within the island by nonlinear effects. The condensation becomes increasingly effective with increasing island width. There is a threshold island width above which there is a decrease in the magnitude of the current required for stabilization, and a second threshold at which the condensation effect is dramatically enhanced, providing efficient stabilization of larger islands than presently contemplated. There is a hysteresis effect above the second threshold that shrinks the island to smaller width. The condensation effect itself also reduces the difficulty of aiming the rf current deposition for accurate radial alignment with the island. These effects reduce the risks associated with the sensitivity of rf stabilization to radial misalignment relative to the island. Given

that disruptions are often preceded by the appearance of large locked modes [83], the improved capability for stabilizing large islands also suggests disruption mitigation via rf control over the associated islands. The condensation effects here are available for LHCD and for ECCD, because of their sensitivity to temperature, but not generally to other current drive methods. To a lesser extent the Ohmic current condenses too (and is stabilizing), but in a strong overdrive mode, the Ohmic countercurrent strongly condenses (and is destabilizing). Signatures of the fundamental, but useful, phenomena predicted here should be observable in more precise temperature measurements in island interiors, through comparisons of different methods of rf current drive, through more careful analyses of saturated island widths, and through comparisons to island formation in the rf overdrive regime.

*Acknowledgments:* The authors would like to acknowledge conversations with Ms. Ge Dong. This work was supported by DOE Contract No. DE-AC02-09CH11466.

---

[1] A. H. Reiman, Physics of Fluids **26**, 1338 (1983).  
 [2] Y. Yoshioka, S. Kinoshita, and T. Kobayashi, Nuclear Fusion **24**, 565 (1984).  
 [3] Z. Chang et al., Phys. Rev. Lett. **74**, 4663 (1995).  
 [4] R. J. LaHaye, L. L. Lao, E. J. Strait, and T. S. Taylor, Nuclear Fusion **37**, 397 (1997).  
 [5] H. Zohm et al., Plasma Phys. Cont. Fusion **39**, B237 (1997).  
 [6] D. A. Gates et al., Nuclear Fusion **37**, 1593 (1997).  
 [7] C. C. Hegna and J. D. Callen, Phys. Plasma **4**, 2940 (1997).  
 [8] H. Zohm, Physics of Plasmas **4**, 3433 (1997).  
 [9] R. Harvey and F. Perkins, Nucl. Fusion **41**, 1847 (2001).  
 [10] Q. Yu, S. Gunter, G. Giruzzi, K. Lackner, and M. Zabiego, Physics of Plasmas **7**, 312 (2000).  
 [11] R. Prater et al., Nuclear Fusion **43**, 1128 (2003).  
 [12] S. Bernabei, A. Cardinali, G. Giruzzi, and M. Zabiego, Nuclear Fusion **38**, 87 (1998).  
 [13] C. D. Warrick et al., Phys. Rev. Lett. **85**, 574 (2000).  
 [14] G. Gantenbein et al., Phys. Rev. Lett. **85**, 1242 (2000).  
 [15] H. Zohm et al., Nuclear Fusion **41**, 197 (2001).  
 [16] A. Isayama et al., Plasma Phys. Cont. Fusion **42**, L37 (2000).  
 [17] R. J. La Haye et al., Phys. Plasmas **9**, 2051 (2002).  
 [18] C. C. Petty et al., Nuclear Fusion **44**, 243 (2004).  
 [19] O. Sauter, Physics of Plasmas **11**, 4808 (2004).  
 [20] R. Kamendje, S. V. Kasilov, W. Kernbichler, I. Pavlenko, E. Poli, and M. F. Heyn, Phys. Plasma **12**, 012502 (2005).  
 [21] R. J. La Haye, Physics of Plasmas **13**, 055501 (2006).  
 [22] R. J. La Haye et al., Nuclear Fusion **48**, 054004 (2008).  
 [23] M. A. Henderson et al., Nucl. Fusion **48**, 054013 (2008).  
 [24] D. De Lazzari and E. Westerhof, Nuclear Fusion **49**, 075002 (2009).  
 [25] F. A. G. Volpe et al., Phys. Plasma **16** (2009).  
 [26] O. Sauter, M. A. Henderson, G. Ramponi, H. Zohm, and C. Zucca, Plasma Phys. Cont. Fusion **52**, 025002 (2010).  
 [27] N. Bertelli, D. De Lazzari, and E. Westerhof, Nuclear Fusion **51**, 103007 (2011).  
 [28] B. A. Hennen, E. Westerhof, P. W. J. M. Nuij, M. R. de Baar, and M. Steinbuch, Nucl. Fusion **52**, 074009 (2012).  
 [29] A. I. Smolyakov, A. Poye, O. Agullo, S. Benkadda, and X. Garbet, Phys. Plasmas **20**, 062506 (2013).  
 [30] B. Ayten et al., Nuclear Fusion **54**, 073001 (2014).  
 [31] D. Borgogno, L. Comisso, D. Grasso, and E. Lazzaro, Physics of Plasmas **21**, 060704 (2014).  
 [32] F. A. Volpe et al., Phys. Rev. Lett. **115**, 175002 (2015).  
 [33] O. Fevrier et al., Plasma Physics and Controlled Fusion **58**, 045015 (2016).  
 [34] S. Wang and Z. W. Ma, Phys. Plasma **22**, 122504 (2015).  
 [35] J. C. Li, C. J. Xiao, Z. H. Lin, and K. J. Wang, Physics of Plasmas **24**, 082508 (2017).  
 [36] D. Grasso, E. Lazzaro, D. Borgogno, and L. Comisso, J. Plasma Phys. **82**, 595820603 (2016).  
 [37] D. Grasso et al., J. Plasma Phys. **84**, 745840302 (2018).  
 [38] N. J. Fisch, Rev. Mod. Phys. **59**, 175 (1987).  
 [39] N. J. Fisch and A. H. Boozer, Phys. Rev. Lett. **45**, 720 (1980).  
 [40] N. J. Fisch, Phys. Rev. Lett. **41**, 873 (1978).  
 [41] R. B. White, D. A. Monticello, M. N. Rosenbluth, and B. V. Waddell, Phys. Fluids **20**, 800 (1977).  
 [42] R. Fitzpatrick, Phys. Plasma **2**, 825 (1995).  
 [43] G. Giruzzi, M. Zabiego, T. Gianakon, X. Garbet, A. Cardinali, and S. Bernabei, Nuclear Fusion **39**, 107 (1999).  
 [44] H. Zohm et al., Plasma Phys. Control. Fusion **49**, B341 (2007).  
 [45] E. Poli et al., Nucl. Fusion **55**, 013023 (2015).  
 [46] R. D. Hazeltine, P. Helander, and P. J. Catto, Phys. Plasma **4**, 2920 (1997).  
 [47] C. F. F. Karney and N. J. Fisch, Phys. Fluids **22**, 1817 (1979).  
 [48] C. F. F. Karney and N. J. Fisch, Nucl. Fusion **21**, 1549 (1981).  
 [49] E. Kolemen et al., Nuclear Fusion **54**, 073020 (2014).  
 [50] E. Lazzaro et al., Plasma Physics and Controlled Fusion **60**, 014044 (2018).  
 [51] F. M. Poli et al., Nucl. Fusion **58**, 016007 (2018).  
 [52] P. T. Bonoli and R. C. Englade, Physics of Fluids **29**,

2937 (1986).

[53] Y. Peysson and J. Decker, *Fusion Sci. Tech.* **65**, 22 (2014).

[54] X. Garbet et al., *Plasma Phys. Control. Fusion* **46**(12B), B557 (2004).

[55] F. Imbeaux, F. Ryter, and X. Garbet, *Plasma Phys. Control. Fusion* **43**(11), 1503 (2001).

[56] C. Mantica et al., *Phys. Rev. Lett.* **102**, 175002 (2009).

[57] J. E. Kinsey et al., *Nucl. Fusion* **51**, 083001 (2011).

[58] V. I. Arnol'd, V. S. Afraimovich, Y. S. Il'yashenko, and L. Shil'nikov, *Bifurcation Theory and Catastrophe Theory* (Springer-Verlag, 1993).

[59] E. Westerhof et al., *Nucl. Fusion* **47**, 85 (2007).

[60] E. Westerhof, *Fusion Sci. and Technology* **61**, 312 (2012).

[61] S. Inagaki et al., *Phys. Rev. Lett.* **92**, 055002 (2004).

[62] K. Ida et al., *Phys. Rev. Lett.* **109**, 065001 (2012).

[63] L. Bardoczi et al., *Phys. Plasma* **23**, 052507 (2016).

[64] N. J. Fisch, *Phys. Fluids* **28**, 245 (1985).

[65] C. F. F. Karney, F. C. Jobes, and N. J. Fisch, *Phys. Rev. A* **32**, 2554 (1985).

[66] Y. Pianroj and T. Onjun, *Songklanakarin J. Sci. Technol.* **34**, 77 (2012).

[67] N. J. Fisch and C. F. F. Karney, *Phys. Rev. Lett.* **54**, 897 (1985).

[68] F. Leuterer et al., *Phys. Rev. Lett.* **55**, 75 (1985).

[69] G. Giruzzi, E. Barbato, S. Bernabei, and A. Cardinali, *Nucl. Fusion* **37**, 673 (1997).

[70] Y. Takase et al., *Phys. Fluids* **30**, 1169 (1987).

[71] Z. Y. Chen et al., *Chinese Phys. Lett.* **22**, 1721 (2005).

[72] B. J. Ding et al., *Phys. Plasmas* **19**, 122507 (2012).

[73] N. J. Fisch, *Journal of Plasma Physics* **76**, 627 (2010).

[74] M. H. Li et al., *Plasma Sci. Tech* **14**, 201 (2012).

[75] N. J. Fisch and C. F. F. Karney, *Phys. Fluids* **24**, 27 (1981).

[76] T. Ohkawa, *Nucl. Fusion* **10**, 185 (1970).

[77] N. J. Fisch, *Nuclear Fusion* **21**, 15 (1981).

[78] G. M. Wallace et al., *IEEE Trans. Plasma Sci.* **44**, 1613 (2016).

[79] B. N. Sorbom et al., *Fusion Eng. Design* **100**, 378 (2015).

[80] N. J. Fisch and J.-M. Rax, *Phys. Rev. Lett.* **69**, 612 (1992).

[81] I. E. Ochs, N. Bertelli, and N. J. Fisch, *Physics of Plasmas* **22**, 082119 (2015).

[82] I. E. Ochs, N. Bertelli, and N. J. Fisch, *Phys. Plasmas* **22**, 112103 (2015).

[83] P. C. de Vries et al., *Nucl. Fusion* **51**, 053018 (2011).